ACCEPTED VERSION

Juan Carlos Pineda Allen, Ching Tai Ng
Debonding detection at adhesive joints using nonlinear Lamb waves mixing

---

PERMISSIONS

https://www.elsevier.com/about/policies/sharing

Accepted Manuscript

Authors can share their accepted manuscript:

24 Month Embargo

After the embargo period

- via non-commercial hosting platforms such as their institutional repository
- via commercial sites with which Elsevier has an agreement

In all cases accepted manuscripts should:

- link to the formal publication via its DOI
- bear a CC-BY-NC-ND license – this is easy to do
- if aggregated with other manuscripts, for example in a repository or other site, be shared in alignment with our hosting policy
- not be added to or enhanced in any way to appear more like, or to substitute for, the published journal article

28 March 2024

---

http://hdl.handle.net/2440/132822

Journal article:

Juan Carlos Pineda Allen, Ching Tai Ng. (2022). Debonding detection at adhesive joints using nonlinear Lamb waves mixing. NDT & E International, 125:102552.

Debonding detection at adhesive joints using nonlinear Lamb waves mixing

Juan Carlos Pineda Allen, Ching Tai Ng[*]

School of Civil, Environmental & Mining Engineering, The University of Adelaide, SA 5005, Australia

Abstract

Many engineering structural elements make use of adhesively bonded joints due to its lighter weight, load distribution and transmission mechanisms. The safety of the structure relies greatly on the condition of the adhesive joint. In this paper, the detection of debonding at the adhesive joint is investigated using a nonlinear Lamb wave mixing approach. The method relies on the presence of combined harmonics as indicative of material nonlinearity due to dislocations or anharmonicity in intact specimens or contact nonlinearity produced by the defects. In this study, experiments and three-dimensional finite element simulations were conducted and demonstrated that the presence of combined frequency wave due to contact acoustic nonlinearity is effective for indicating debonding. The effect of the debonding width was investigated and the debonding width was found to correlate well with the combined harmonic energy generated due to debonding. The findings presented in this study provides physical insights into the effect of debonding mechanisms at adhesive joints in related to the nonlinear Lamb wave mixing approach, and can be used to further develop the debonding detection techniques using wave mixing.

---

[*] Corresponding author: alex.ng@adelaide.edu.au

1. INTRODUCTION

Layered materials have been commonly used in engineering structures such as aerospace, automotive and civil structures. Adhesive joint is one of the commonly used approaches to manufacture layered structural elements [1] [2] and conduct repairs and reinforcement where light weight is of paramount concern [3]. This type of joint has the advantage of avoiding stress concentration by uniformly distributing the stresses. Lighter weights can also be achieved as compared to traditional mechanical joints. The performance of layered materials greatly relies on the adhesive layer. In the manufacturing process, this layer is susceptible to air inclusions or weak bonding strength. During service stage, delamination or debonding caused by impact or fatigue could lead to catastrophic failure of structures. These manufacturing defects and structural damage are not always visible and hard to be detected by visual inspection, therefore, non-destructive testing techniques were developed to inspect and detect these defects and damages without the need to dismantle the real structure.

In many applications, ultrasonic non-destructive testing methods have advantages compared to other non-destructive testing methods as they possess the ability to mechanically probe the defect. Moreover, ultrasonic guided waves have the potential of being suitable for in-situ inspection and monitoring of plate-like and pipe structures. Ultrasonic piezoelectric wafer transducers can be permanently installed on structures and the inspection and monitoring process do not affect operation of the structures and do not require the presence of a technician for on-site operation [4] [5] [6].

1.1 Nonlinear phenomena of ultrasonic guided waves

Linear ultrasonic techniques can be used to detect micro-scale defects and damages, such as local bonding degradation, distributed micro-cracks, and delamination. Nonlinear ultrasonics has the advantage that is more sensitive to smaller size of damage and can detect damage at an earlier state [7]. Detection of these defects and damages are critical for safety inspection and providing early warning. Nonlinear ultrasonics has attracted considerable attention [8] in the past years. This approach relies on nonlinear acoustic phenomena, where nonlinear responses of ultrasonic wave, e.g. higher order harmonics, are generated due to interaction between the incident wave and discontinuities. Higher order harmonic generation can be induced by material nonlinearity due to dislocations or anharmonicity in intact specimens [9] [10] or contact acoustic nonlinearity (CAN) produced by defects [11] [12] [13].

Second order harmonic (or simply second harmonic) generated due to material nonlinearity was proven to be capable of detecting microstructural changes, such as plasticity [14] and mechanical fatigue [15] in metallic specimens, and thermal fatigue damage in composites laminates [16]. CAN was investigated for detecting fatigue cracks in metals [17], delamination in composites laminates [18] [19] and debonding in adhesive joints [20] as well as in FRP-retrofited concrete structures [21]. Adhesive nonlinearity may also generate contact nonlinearity [22].

Despite recent advances, some limitations remain challenging for second harmonics generation techniques. The nonlinearities induced by contact between the structure components under inspection and the ultrasonic transducer can mask the damage-related and material nonlinearities. Secondly, the relatively small magnitude of the higher harmonic is hard to be measured accurately. Lastly, nonlinearities are also introduced by the testing equipment compromising the isolation of the source of the nonlinearity.

To overcome these drawbacks, the wave mixing method utilizing two ultrasonic waves at different single central frequencies has been developed in last few years [23] [24]. Wave mixing method can be primarily classified as collinear [25] and non-collinear [26] depending on the wave propagation angle between the incident waves. Foreseeing its advantages, mixed-frequency response is the focus of this paper.

1.2 Nonlinear mixed-frequency response

Jingpin *et al*. employed collinear wave mixing of bulk waves to study inter-granular corrosion [27] and micro-crack [28] in steel specimens. They also investigated bulk shear wave mixing and non-collinear wave mixing to determine the presence of fatigue cracks [29]. Two-dimensional finite element (FE) method was applied to demonstrate the potential of non-collinear mixing method in detecting closed cracks using bulk shear waves [30]. A time and frequency domain analysis of a slender beam was used to determine crack location with the consideration of dispersion characteristics [31]. Croxford *et al*. [26] employed bulk waves to characterize material nonlinearity due to fatigue and plasticity damage using the non-collinear method. Material nonlinearity was experimentally correlated to plastic deformation of aluminium alloy. An independent nonlinear acoustic parameter using collinear wave mixing of bulk waves, which is strictly related to plastic deformation, was introduced and validated numerically and experimentally [32]. Further experimental studies demonstrated that the collinear method can also measure localized plastic deformation [33]. The bulk waves employed in the aforementioned studies are limited to a very localized inspection area.

Compared to ultrasonic bulk waves, guided waves (Lamb waves) offer advantages such as the ability to inspect inaccessible locations. Specific wave modes can be appropriately selected and generated, even though mainly the fundamental modes were used in long range measurements. Their applications to submerged elements or structures with one side exposed to fluids were investigated [34] [35] [36], although to date, viscoelasticity constraints and the Cremer's correspondence principle still limit its further development.

Collinear and non-collinear plane wave mixing was investigated by Hasanian *et al*. [37] [38]. Ishii *et al*. [39] theoretically analysed nonlinear wave propagation in an homogenous and isotropic plate. They elucidated the non-collinear interaction of monochromatic plane waves employing a perturbation analysis and infinite beam widths. They also conducted FE analysis considering finite beam width and time durations to gain further understanding on the scattered wave generation. Further studies were carried out to advance understanding of counter-propagating guided waves [40] [41]. Li *et al*. [42] studied mixed-frequency response induced by collinear co-directional Lamb waves and predicted the generation of second and third order combined harmonics. They also investigated impact damage detection [43]. Codirectional Lamb wave mixing was used to investigate micro crack [44] and localized creep detection in steel plates [45] and thermal related microstrural changes in aluminium plates [46]. Distributed micro-cracks were also investigated using codiredirectional Lamb wave mixing and FE modeling [47].

For the two aforementioned higher harmonic generation mechanisms, CAN is the focus in this paper. It has potential to detect debonding in layered structures using wave mixing technique. Different to finding triplets and exploring the cumulative nature of the secondary wave as in [43] [47] [48], we numerically and experimentally investigate CAN due to the clapping mechanisms at the debonded layer when Lamb wave propagates through the plate and generates combined harmonic, and hence, the internal resonance conditions are not assesed in this paper.

1.3 Damage detection of adhesive joints using guided waves

The applications of linear Lamb waves for detecting damage in adhesive joints were initially employed to study lap shear joints [49] and explored the use of the anti-symmetric (A_0) mode of Lamb wave for characterization due to its sensitivity and dominant out-of-plane displacement over its in-plane displacement [50]. Some other studies investigated the use of root-mean-square and non-contact sensing for damage imaging of adhesive joints [51]. The contact phenomenon was investigated for detecting delamination in composites laminates

using time domain signals and mode conversion features [52]. Wavenumber analysis was employed to locate and quantify delamination based on trapped energy from the wave [53]. However, these studies only focused on the linear Lamb waves.

More recently, nonlinear guided waves were used to identify the existence of delamination across different plies in composite beams [19]. Yelve *et al*. [18] employed a spectral damage index to correlate with delamination size and a time-frequency method to further determine delamination location. But these studies only focused on higher harmonics generated due to single frequency wave interacting with CAN.

Existing studies focusing on wave mixing phenomenon of adhesive bonds [54] [55] [56] were limited to the bulk wave. However, bulk wave interaction is different to wave interaction in plate-like structures as pointed out by de Lima *et al*. [57] and Hasanian *et al*. [37]. Therefore, our study is to investigate a different type of wave mixing, specifically guided waves as their interaction has not yet been fully understood. To date, research on Lamb wave mixing techniques is still very limited, in particular, the Lamb wave mixing phenomenon at debonding in layered materials needs to be investigated. The objective of this paper is to investigate the Lamb wave mixing for detecting local debonding at adhesive joints using three-dimensional (3D) FE simulation and experiment. Debonding detection remains a challenging area in the non-destructive testing community given that debonding (and alike) defects mostly locate under the surface of the structural component, deriving in long inspection times if inspected with traditional point-to-point ultrasonics. By using ultrasonic guided waves, the time of inspection can be reduced as the inspection can be more effective due to the relatively long propagation inspection distance of guided waves. This can minimize labour related costs. The experimental and numerical studies conducted in this paper help gain insight into the combined harmonic generation due to guided wave mixing and interaction with debonding. It further demonstrates that the combined harmonic wave generation due of wave mixing and interaction with debonding can be reliably measured in experiments. Unlike most research in guided wave mixing to date where simplified plane strain models were used, the 3D FE model in this paper ensures the characteristics of the wave can be fully captured and well correlated to the experimental data. The findings of this study help further advance the use of wave mixing for damage detection and characterization.

This paper is organized as follows. Section 2 introduces the Lamb wave mixing phenomenon. Section 3 presents the experimental framework, where the specimen preparation and actuating/sensing set up are described. The theoretically and experimentally obtained dispersion curves are compared and validated. Section 4 describes the details of the FE

simulation. The FE model is validated theoretical and experimentally in this study. In Section 5, a series of case studies on Lamb wave mixing and interaction with debonding are presented experimentally and numerically. The effect of debonding size on combined harmonic wave generation is investigated in Section 5. Finally, conclusions are presented in Section 6.

2. LAMB WAVE MIXING PHENOMENON

When two or more propagating waves with different central frequencies interact with a linear system, only incident frequencies will exist in the frequency spectrum of the response. However, when interacting with a nonlinearity source (damage or material related), the total response comprises a linear response, higher harmonics and combined harmonics. This is schematically represented in Fig. 1. For a linear system, the frequency spectrum u of the time domain response only contains the incident frequencies f_a and f_b. Conversely, the spectrum of the response after interaction with a nonlinear system additionally contains higher harmonics $2f_a$ and $2f_b$, and combined harmonics f_b-f_a and f_a+f_b.
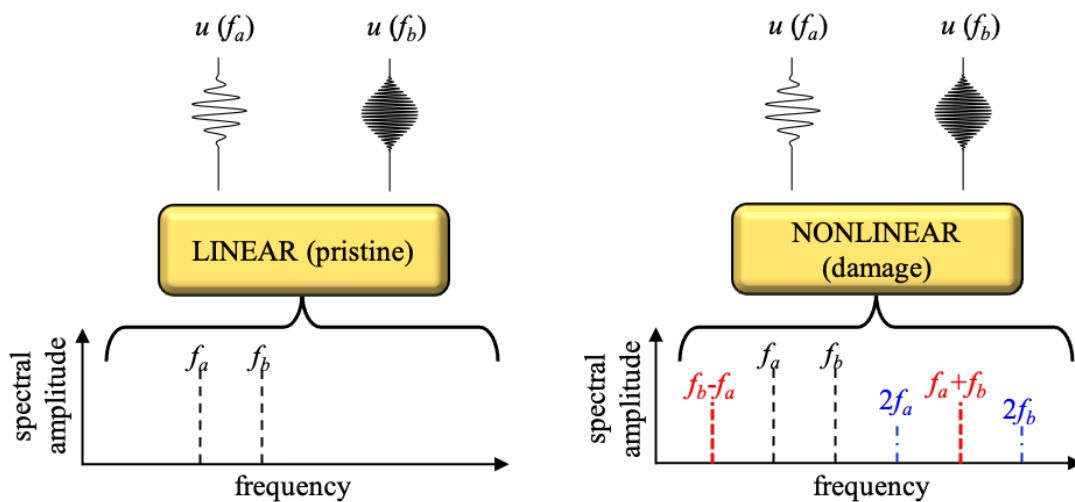

Fig. 1. Schematic representation of wave-mixing phenomena in linear and nonlinear system

The existence of combined harmonics, specifically the combined frequency wave at the sum harmonic frequency for collinear Lamb wave mixing, and its sensitivity to damage in adhesive joint are experimentally and numerically investigated in this paper. In the rest of the paper, the combined frequency wave at the sum harmonic frequency refers to combined frequency wave unless there is a specific indication on the frequency.

3. EXPERIMENT

3.1 Specimen description

Specimens used in this study consist of three layers of elements, which are two grade 6061-T6 aluminium plates and one epoxy layer. The dimensions of the two aluminium plates are 300mm×100mm×1.02mm and 300mm×100mm×1.60mm. The plates were cleaned with acetone to remove any impurities and oil, and then, treated with sandpaper and cleaned with acetone again to remove any dust before applying the epoxy resin to bond them together. The epoxy is a two-part adhesive glue MBrace 4500. Distributed weights were placed on the top of the specimen to ensure equal pressure was applied in the drying process. Although it is difficult to control rigorously the thickness of the glue layer during the curing process, an average thickness of 0.20mm was obtained once the epoxy layer fully dried and hardened. A digital calliper was used to measure the total thickness of the specimen every 50mm all around its perimeter.

Three specimens were prepared. One of the specimens was fully bonded, and the other two specimens have debonding and were prepared as follows. For the second specimen, the epoxy resin was not applied to a strip area of approximately 10mm wide and parallel to the shorter side of the plate in order to create a weak bonding in the specimen after the top and bottom plate were bonded together. For the third specimen, a 10mm wide Mylar strip was inserted during the epoxy resin application. In the second and third specimens, both modifications were done at the centre of the longer side of the specimens as schematically shown in Figure 2. The purpose of the Mylar insert and the epoxy absence is to create a weak bonding region in the specimens. To induce debonding at the weak bonding region, a three-point bending test under cyclic load was conducted. The bottom plate on the support is a 1.02mm thick plate while the top plate is 1.60mm thick. The load was applied on the top surface of the top plate so that the epoxy resin layer was subjected to tensile stress during the bending test.
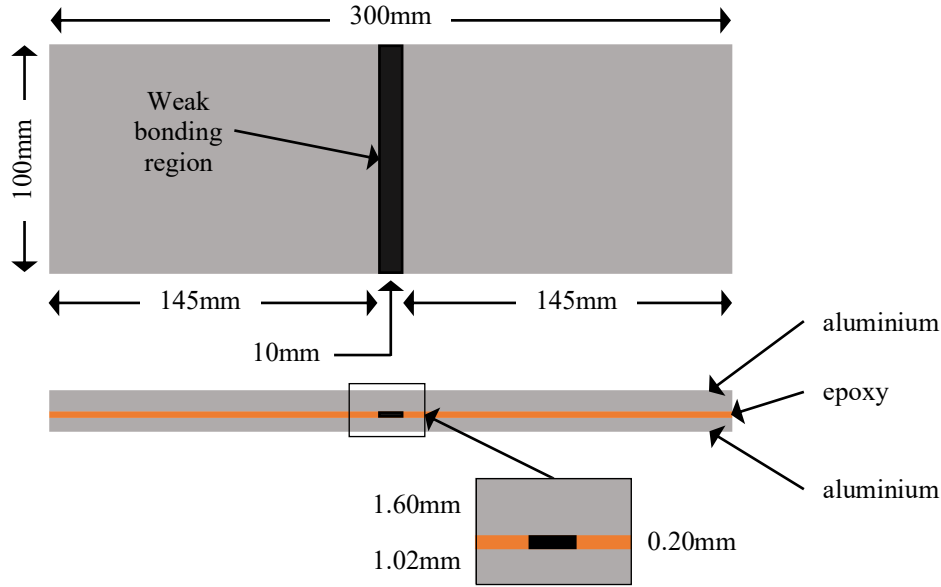
Fig. 2. Schematic diagram of the adhesively bonded specimen

3.2 Equipment setup

A wedge made of Teflon was designed and used with a transducer to generate A_0 Lamb wave. Longitudinal velocity of the Teflon is 1336.37 m/s, the incident angle is calculated using Snell's law. A number of different wedges and two different contact transducers, ULTRAN GC200-D13 and GC350-D13, were used in the experiment. A special fixture was 3D-printed to assemble the transducer to the wedge as shown in Figure 3. Light motor oil was applied at the wedge-specimen interface and the wedge was fixed on the top of the specimen by a clamp. Reflective paint was applied to the specimen surface to increase the optical backscatter reflection of the laser beam. The measured signals were averaged 1000 times and passed through a low-pass filter to increase the quality of the measurements. The signal averaging was to improve the signal to noise ratio by minimizing the measurement white noise. A one-dimensional (1D) scanning Laser Doppler Vibrometer (SLDV) was used to measure the displacement response of the wave. Even though the 1D SLDV could possess a limitation in capturing a symmetric wave mode, previous studies showed the amplitude of the symmetric wave mode generated due to debonding type of damage is usually weak. For practical application, piezoceramic transducers can be used to measure the wave signals. However, this study aims at investigating the wave mixing phenomenon so the 1D SLDV was used to provide enough flexibility on the measurement location, and hence, the wavenumber-frequency analysis can provide further understanding on the wave phenomenon. A PC-controlled NI PXI-5412 arbitrary function generator was used to generate the incident pulse. The signal was then

amplified by a CIPRIAN HVA-800-A amplifier. Figure 4 shows the experimental setup used in this study.
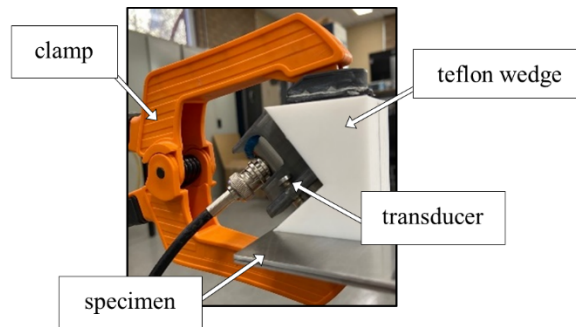

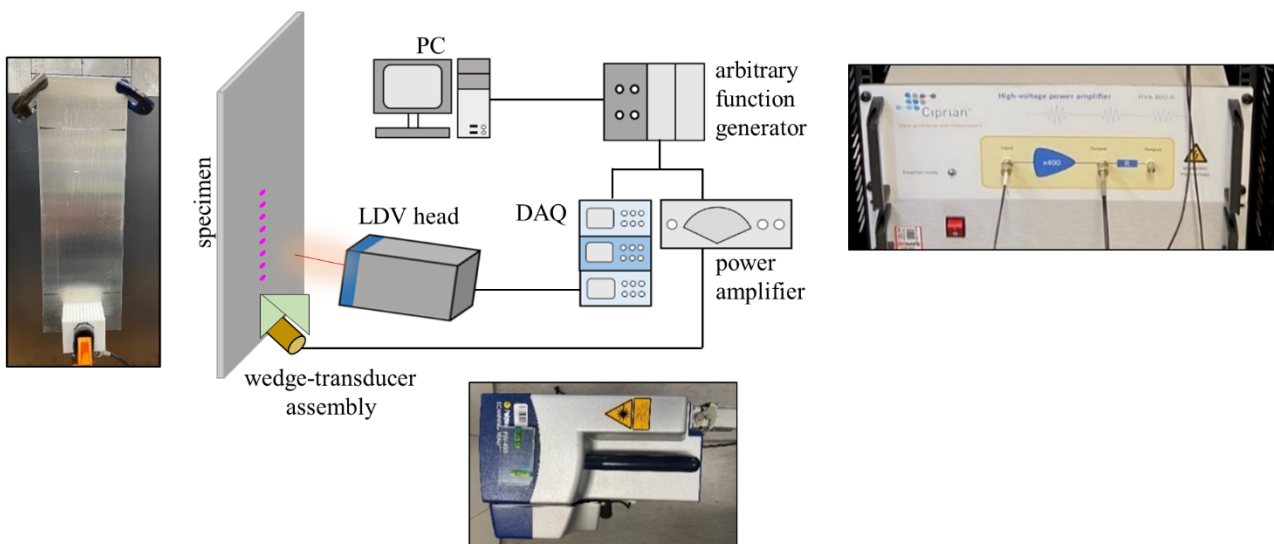Fig. 3. Wedge-transducer-specimen assembly

Fig. 4. Schematic diagram of the experimental setup

3.3 Experimentally measured dispersion curves

A number of tests were first conducted to validate the dispersion curves with theoretical solutions. The fully bonded specimen was used in the tests. Eight independent sinusoidal tone-burst pulses with different central frequencies ranging from 150 kHz to 500 kHz in steps of 50 kHz were excited and a line scan of 41 consecutive points with 1mm distance between points was conducted for each excitation frequency. Eight different wedges corresponding to the eight different phase velocities were used. Each wedge was designed using the corresponding Snell's angle, which are 57°, 50°, 46°, 43°, 41°, 39°, 38° and 37° for the 150 kHz, 200 kHz, 250 kHz,

300 kHz, 350 kHz, 400 kHz, 450 kHz and 500 kHz pulses respectively. Out-of-plane displacement response of the specimen was measured for each line scan and recorded for further processing. Frequency-wavenumber (f-k) by means of two-dimensional Fourier transform algorithm and frequency-group velocity (f-c_g) were calculated for each of the tests. For a Lamb wave propagating on plate along the x direction, the displacement on the surface can be described by the general analytical expression [58],

$$u(x,t) = A(\omega)e^{i(kx - \omega t - \varphi_0)} \tag{1}$$

where A is the amplitude, ω is the angular frequency, φ_0 is the phase. The wavenumber k is given by $k = \omega/c_p$, for a wave with phase velocity c_p. The two-dimensional transform is given by,

$$H(k,f) = \int \int u(x,t)e^{-i(kx - \omega t)}dxdt \tag{2}$$

In most of the measured Lamb wave signals, more than one propagating Lamb mode exist and travel simultaneously, which hinders the straightforward calculation of phase and group velocity. The graphical representation of the two-dimensional Fourier transform helps identify different propagating modes and it needs data measured at multiple measurement locations. We employed the laser scanning vibrometer to achieve non-contact measurement of the Lamb wave signals at multiple measurement points. The group velocity was calculated using the time-of-flight of the signal envelope obtained from the Hilbert transform and distance between consecutive measurement points. Theoretical dispersion curves were calculated using DISPERSE under the assumption that the wavefront is an infinite plane and normal to the direction of wave propagation. Material properties used to calculate dispersion curves of the epoxy and aluminium are density $\rho_e = 1200 \, kg/m^3$ and $\rho_a = 2704 \, kg/m^3$, Young's modulus $E_e = 3.70 \, GPa$ and $E_a = 69 \, GPa$, and Poisson's ratio $\nu_e = 0.40$ and $\nu_a = 0.33$, respectively. A contour plot of the calculated frequency-wavenumber array and group velocity values for the fully bonded specimen are shown in Figure 5, where the theoretical values are represented by continuous black lines. A_0, S_0, and higher order modes are not antisymmetric or symmetric because the specimens are not symmetric in the thickness direction. Given the accepted terminology in the existing literature, the authors keep the terms "A" and "S" for the antisymmetric and symmetric modes of Lamb waves, respectively.
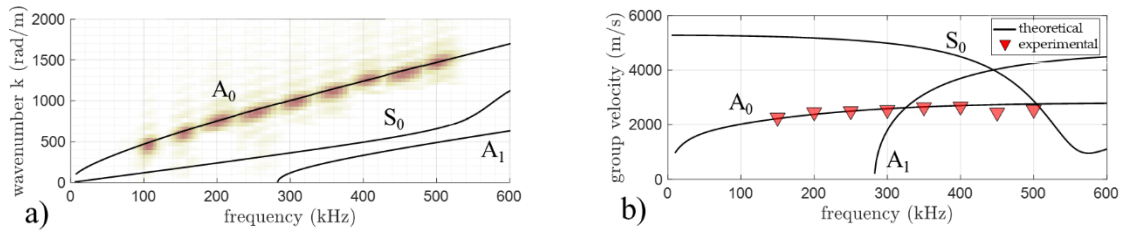
Fig. 5. Experimentally obtained and theoretically calculated a) frequency-wavenumber and b) group velocity dispersion curve

4. 3D FINITE ELEMENT SIMULATION

4.1 Model description

A 3D FE model was developed to simulate the mixed frequency Lamb wave propagation. Although a one-dimensional model has less computational cost, a 3D FE model was employed in this study to ensure the FE prediction is highly accurate, in particular capturing the wave attenuation effect in the wave propagation and the non-plane wavefront effect of the generated wave. The FE model is experimentally verified and used to gain physical insights into the wave mixing phenomena and interaction with the debonding. The model has three layers, whose top and bottom layer are grade 6061-T6 aluminium plate and mid layer is an epoxy layer with density $\rho = 1200 \, kg/m^3$, Young's modulus $E = 3.70 \, GPa$ and Poisson's ratio $\nu = 0.40$. Even though a nonlinearity coefficient beta is of the same order for the epoxy and aluminium, a linear behaviour of the epoxy layer was assumed because the epoxy layer is thin as compared to the aluminium layers. The assumption was further corroborated when validating the FE model results and the experimental results. Eight-noded brick elements, C3D8R, with each node having three translational degrees-of-freedom and reduced integration were used [59]. The maximum element size was set to 0.20mm to ensure there are at least 20 elements within the shortest wavelength of interest. There are five element layers for the 1.02mm thick aluminium plate, two element layers on the epoxy and eight element layers for the 1.60mm thick plate. The increment time step was automatically controlled by ABAQUS/Explicit. Mechanical constitutive behaviour based on the nonlinear strain energy function of Murnaghan was modelled in ABAQUS/Explicit through a VUMAT subroutine to simulate the material nonlinearity [60]. The material properties of the plates are listed in Table I. Adhesive bond between aluminium layers and epoxy layer is assigned by using tie constraints.

Table I. Material properties used in the FE simulations [61]

Density (kg/m³)	E (GPa)	v	l (GPa)	m (GPa)	n (GPa)	λ (GPa)	μ (GPa)
2704	69	0.33	-281.50	-339.00	-416.00	54.30	27.30

4.2 Absorbing layers

Absorbing layers by increased damping (ALID) was implemented in the FE model to avoid the wave reflected from the edges of the plate. ALID contains layers with increasing value of damping so that the energy of the Lamb wave is gradually absorbed when approaching the ALID at the edges of the plate. This significantly reduces the computational cost of the FE simulations, and hence, the model is computationally efficient for investigating the Lamb wave propagation and interaction at the debonding. The ALID was modelled at all perimeters of the plate. The ALID have 100 layers, each has 0.5mm wide, making the total width of the ALID to be 50mm. In this study, mass proportional damping was used to model the ALID. The damping value of at each ALID layer is obtained by the following power-law formulation [62]:

$$C_M(x) = C_{max} \times X(x)^P \tag{3}$$

where x is the location between the edge of the plate without the ALID and the ALID itself, $P = 3$ and $C_{max} = 2.5 \times 10^6$. The total in-plane dimensions of the model with the ALID is 400mm×250mm.

4.3 Numerically calculated dispersion curves

A_0 Lamb wave is excited by applying out-of-plane nodal displacement at the top and bottom nodes in a region of the transducer. Firstly, eight simulations with the identical FE model but different central frequencies of the incident pulse were used. Each incident signal is a Hanning-windowed tone burst pulse with central frequency ranging from 150 kHz to 500 kHz in steps of 50 kHz. Out-of-plane displacement response u_t at the top surface of the three-layered plate model was calculated at 41 consecutive points with 1mm spacing. Frequency-wavenumber (f-k) and frequency-group velocity (f-c_g) were calculated for each of the simulations. A contour plot of the FE calculated frequency-wavenumber and group velocity values are shown in Figure 6, where the theoretical values are represented by continuous black lines.
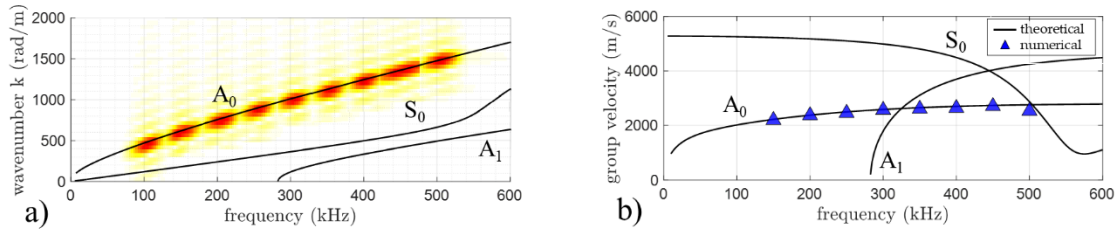
Fig. 6. Numerically and theoretically calculated a) frequency-wavenumber and b) group velocity dispersion curve

The results confirm the dispersion characteristics of the FE model of the fully bonded specimen are able to represent the A_0 Lamb wave propagation. Due to the multi-modal characteristics of Lamb waves, the use of the fundamental modes below the cut-off frequency is preferred. In this study, the cut-off frequency is 285 kHz. Research demonstrated that incident antisymmetric Lamb waves have great sensitivity to delamination [19], debonding [63] and low velocity impact damage [64] given its quasi-flexural propagation nature. They also have better capability of detecting small discontinuities in the propagating media given their shorter wavelengths comparing to symmetric Lamb waves at the same frequency. Therefore, incident A_0 mode was chosen in this study to explore the interaction of the antisymmetric Lamb wave with the local debonding.

5. EXPERIMENTAL AND NUMERICAL WAVE-MIXING CASE STUDIES

Ten case studies were carried out experimentally and numerically. Different specimens, FE models and excitation frequencies were considered in these case studies. The purpose of these case studies is to explore the feasibility and reliability of using wave mixing approach for detecting debonding in layered structures. The case studies are summarized in Table II. Case E1 considered a fully bonded specimen under A_0 incident Lamb waves with frequencies 150 kHz and 250 kHz, named f_a and f_b, respectively. In Case E2, 200 kHz and 300 kHz were used as excitation frequencies for the fully bonded specimen. Case E3 considered a specimen with debonding, and 150 kHz and 250 kHz excitation frequencies. Case E4 used the same specimen, but the excitation frequencies were 200 kHz and 300 kHz. The remaining specimen with debonding was used in Cases E5 and E6, which consider different excitation frequencies. Fully bonded FE model was used in Cases N1 and N2. Cases N3 and N4 considered FE models with a debonding.

To model the debonding, tie constraints were removed between the aluminium and epoxy layer along a 10mm width strip parallel to the shorter side of the model. To avoid interpenetration between debonded surfaces so that the CAN effect can be simulated, a hard contact and surface-to-surface contact interaction is implemented in the FE model. The strip was located at the centre of the plate. The incident signal consists of a tone burst pulse composed of two sinusoidal pulses with different central frequencies, or in other words, two sinusoidal tone burst pulses with different central frequencies were created separately and then merged to generate a single excitation signal. The number of cycles of the excitation signals was selected so that the durations of the pulses are the same, they are 8 cycle for 150 kHz, 13 cycle for 250 kHz, 10 cycle for 200 kHz and 15 cycle for 300 kHz. The mixing zone is approximately 86mm. Frequencies selection was based on two main reasons, on the one hand to take advantage of the operative frequency bandwidth of the used transducers, and on the other hand, such as the combined frequency wave was not multiple of any of the input frequencies. Since generated signals have different group velocities, further numerical simulations, which are not presented in this paper, have indicated they are separated at approximately 450mm. For the additional simulations, an 8-cycle 150 kHz pulse was actuated first, then an independent 13-cycle 250 kHz pulse, and lastly both pulses concomitantly.

Table II. Experimental and numerical Lamb wave mixing case studies

| | Case | Specimen | Incident frequencies | |
			f_a (kHz)	f_b (kHz)
Experimental Study	E1	fully bonded	150	250
	E2	fully bonded	200	300
	E3	debonded (mylar inserted at debonding region)	150	250
	E4	debonded (mylar inserted at debonding region)	200	300
	E5	debonded (no epoxy applied at debonding region)	150	250
	E6	debonded (no epoxy applied at debonding region)	200	300
Numerical Study	N1	fully bonded	150	250
	N2	fully bonded	200	300
	N3	debonded	150	250

	(untied constraints at epoxy layer in the debonding region)		
N4	debonded (untied constraints at epoxy layer in the debonding region)	200	300

A similar experimental setup used in the previous section was employed for the wave generation and data acquisition (Figs. 3 and 4). However, different set of wedges were used in this section. A 52° Teflon wedge with the GC200-D13 transducer actuated the 8-cycle 150 kHz and 13-cycle 250 kHz pulse. In contrast, the GC350-D13 transducer with the 46° Teflon wedge was used to actuate the 10-cycle 200 kHz and 15-cycle 300 kHz pulse. Wedges were chosen considering either (a) the average angle of the two Snell's angles of the two incident frequencies, or (b) the Snell's angle corresponding to the average frequency value of the two incident frequencies. Using the SLDV, the out-of-plane displacement was measured at a point located 60mm from the centre of the debonding region in the forward propagating direction. To improve the signal-to-noise ratio, the measured signals were averaged 1000 times and pass through a low-pass filter. The signal averaging is to improve the signal to noise ratio by minimizing the measurement white noise. In the FE model, top out-of-plane displacement for nodes located at 60mm from the debonding centre in the forward propagating direction were calculated. A snapshot of the displacement response of the FE model with debonding when the incident A_0 Lamb wave interacts with the debonding (Case N3) is shown in Figure 7a. The figure also shows a zoom-in of the cross-section along the Z axis at the debonding region. To investigate the harmonic generation in the measured signals from the experiments and FE models, the Fast Fourier Transform was used to transfer the data from time domain to frequency domain for all cases (Cases E1 to E6 and N1 to N4), and the results are shown in Figure 9.
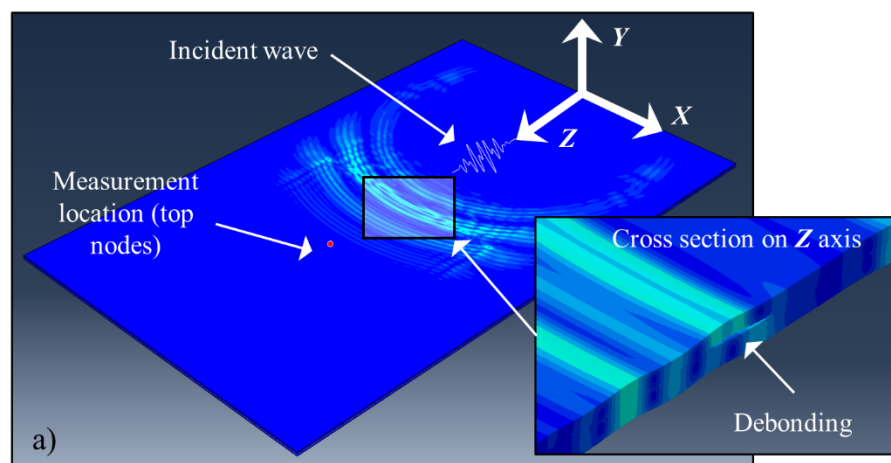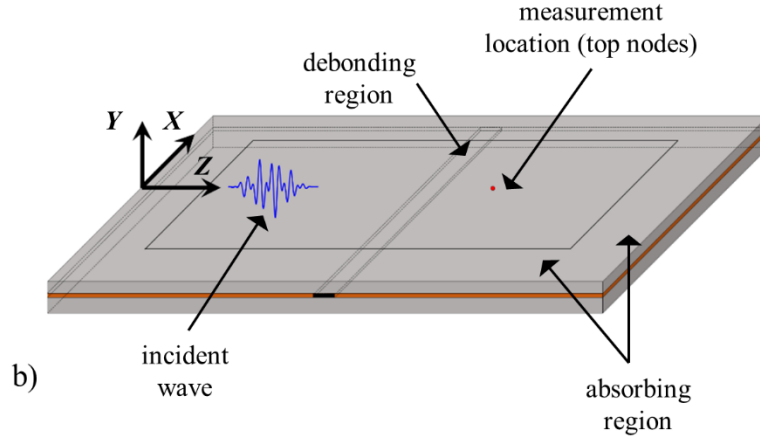
Fig. 7. a) Snapshot of the A_0 Lamb wave interacts with debonding, b) Schematic layout of the debonding plate with debonding

Two preliminary numerical cases (not listed in Table II) were first conducted to confirm the combined frequency wave is A_0 mode, one case for the fully bonded model and the other case for the debonded model. The out-of-plane displacement for a total of 41 points separated every 1mm were calculated. In Fig. 8, the frequency-wavenumber curves for the two cases are shown. It is noted that the generated combined frequency wave due to debonding corresponds to the A_0 mode as expected.
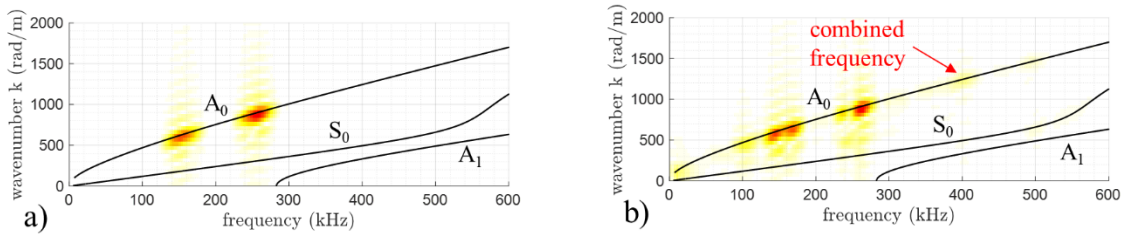

Fig 8. Frequency-wavenumber a) fully bonded, b) debonded

We continue the study with the cases listed in Table II. Fig. 9a shows the spectral content of incident frequencies at 150 kHz and 250 kHz. The results show that additional frequency components appear for signals obtained from the debonded specimens in experiment and FE simulation. Higher harmonics and combined harmonics, including the combined frequency wave f_a+f_b can be observed. These harmonics can be associated with material nonlinearity and nonlinearity generated by CAN. However, CAN-induced harmonics by debonding are expected to be much larger than material nonlinearity-induced harmonics [7] [65]. Similar phenomenon is observed in Fig. 9b when 200 kHz and 300 kHz were the central frequencies of the incident wave signal, which reveals the frequency components at 500 kHz.

The combined frequency wave at the difference harmonic frequency is also observed, mostly for the 200 kHz and 300 kHz pulse. This is not obvious for the 150 kHz and 250 kHz pulse, as the combined frequency at the difference harmonic frequency is masked by the 150 kHz component.

The results indicate that mixed frequency response is effective for local debonding detection at adhesive joints, which do not have any obvious visual evidence on the surface as it is internal damage. The results show that there is good agreement on the experimentally measured and numerically calculated combined frequency wave induced by the debonding. Therefore, the 3D FE model can provide reasonable accuracy in predicting the combined frequency wave in wave mixing.
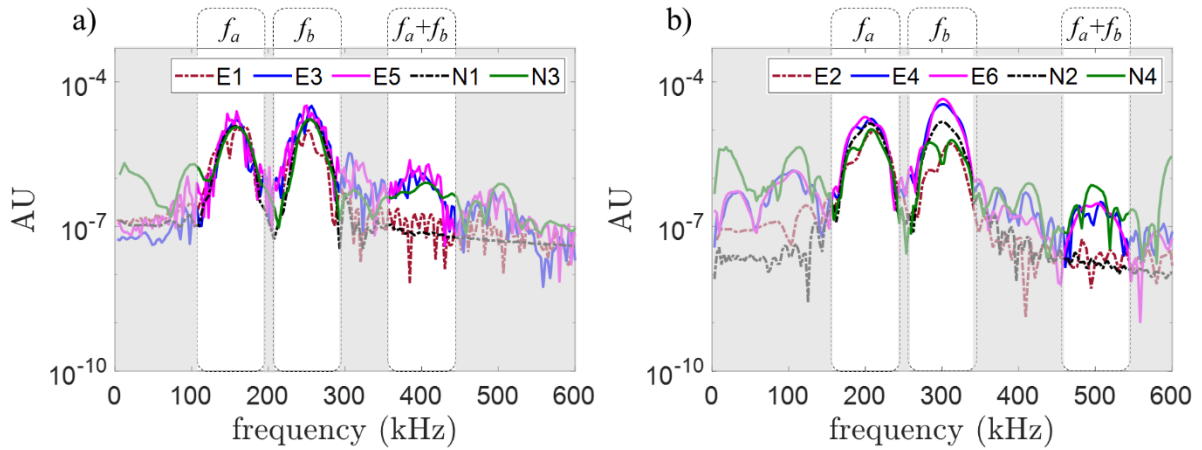

Fig. 9. Experimental measured and numerically calculated Fourier spectra for a) 150 kHz and 250 kHz, and b) 200 kHz and 300 kHz incident frequencies

6. EFFECT OF DEBONDING SIZE

In this section, the experimentally verified FE model was used to provide a parametric study to investigate the effect of debonding size on the combined harmonics. Sixteen cases with different debonding length-to-wavelength ratios, d/λ, were considered. They are summarized in Table III and a schematic diagram is shown in Figure 7b. λ is the wavelength of the combined frequency wave of the A_0 Lamb wave. The centre of the debonding region is located at 100mm from the excitation location, and the measurement points are located at 60mm from the debonding centre in the z direction.

Table III. Summary of debonding length-to-wavelength ratios considered

d/λ	0.125	0.250	0.375	0.500	0.625	0.750	0.875	1.000
d/λ	1.125	1.250	1.375	1.500	1.625	1.750	1.875	2.000

Frequency pair of 150 kHz and 250 kHz was selected in this study. Out-of-plane nodal displacements at the top of the model were calculated for each of the simulations. A typical time domain response for the cases of models having a debonding with d/λ=1.00 and d/λ=2.00, and fully bonded model are shown in Figure 10a. The corresponding frequency spectra are shown in Figure 10b. It can be observed that the response is distorted due to the debonding. Additionally, a shift in energy content from the incident wave to the generated pulse within the debonding is expected from the observation of the maximum displacement. The time-frequency analysis in Figure 11 also reveals information of the combined harmonics.
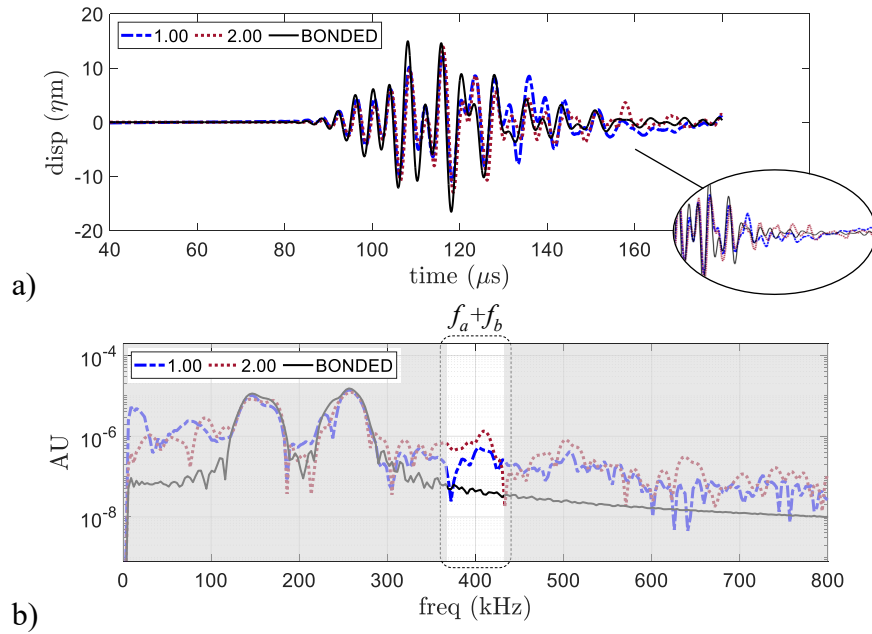

Fig. 10. Typical a) time domain and b) frequency spectra of
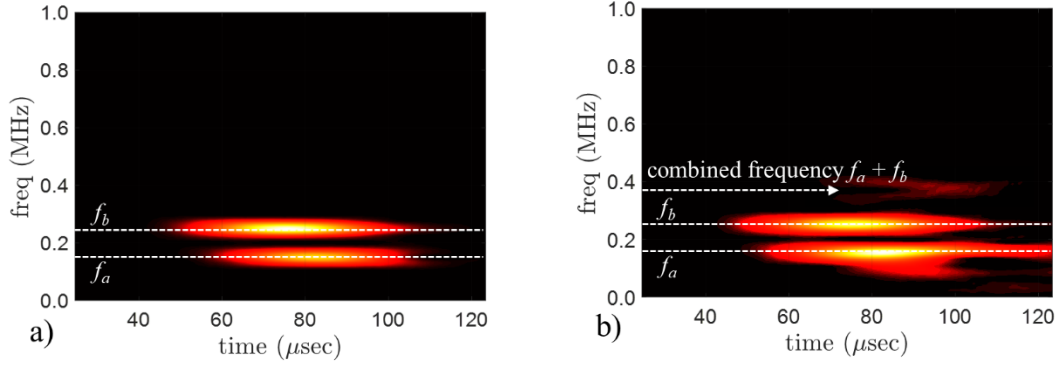displacement responses measured at 60mm from debonding region

Fig. 11. Time frequency spectrum for a) the case with d/λ=2.00 debonding and b) fully bonded specimen

Previous research investigated time domain features of the response to analyse contact mechanisms in composites laminates [52] [66]. However, analyses were conducted using single frequency pulses with the mode conversion phenomenon. The converted modes are able to travel long enough distances and the newly converted modes can separate from the incident waves once it interacts with the damage. However, for mixed-frequency analyses, the effect in time domain becomes more complicated which deserves a separate and dedicated study. Once the incident wave containing f_a and f_b reaches the debonding, f_a+f_b and f_b-f_a are generated. However, part of these newly generated waves travel back to the debonding location and interact with the damage, and again propagate in both forward and backward direction. This backward and forward process is repeated multiple times, so the waves contain multiple frequencies components at incident and combined frequencies. This effect can also be observed in the frequency domain in Figure 10b, where spectral contents for d/λ=1.00, d/λ=2.00 and the fully bonded model are plotted.

Given the difficulty in analysing time domain features with respect to debonding size due the aforementioned reasons, the Fourier spectrum was used in this study. As explained before, multiple reflections occur at the debonding location, but the transmitted energy content could be an indicator of the extent of the debonding. This idea is further implemented by calculating the area under the Fourier amplitude spectrum and then it is correlated with the debonding region. Area under the curve was calculated using the trapezoidal rule for a frequency band equivalent to that of the input frequencies.
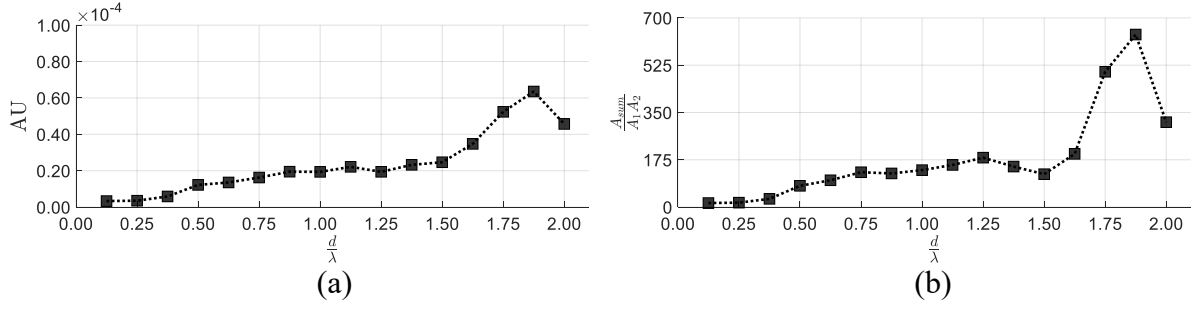
Fig. 12. a) Transmitted energy and b) nonlinear parameter $A_{sum}/A_1 \times A_2$ in relation to debonding length-to-wavelength ratios

Figure 12a shows the relationship between d/λ and energy calculated for the sixteen debonding to wavelength ratios. The responses are nodal displacements located at 60mm of the top of the model from the debonding centre in the forward propagating direction. A steady increasing trend is observed from $d/\lambda=0.125$ to $d/\lambda=1.000$, but the trend then decreases and fluctuates right after $d/\lambda=1.125$ and greater d/λ ratios. It is because when the debonding width increases, the overall contact area also increases and generates more energy when the wave excites and travels through the contact area. For greater values of d/λ, however, the wavelength of the generated wave at the combined frequency wave is shorter than the debonding width. Even though the contact area increases, the effect of the overall contact area is not necessarily correlated to the energy that is generated by the contact effect for d/λ greater than 1.125.

A nonlinear parameter $A_{sum}/A_1 \times A_2$ is then calculated, where the amplitude of the combined frequency wave, A_{sum}, is divided by the product between amplitudes at the incident frequencies A_1 and A_2, and plotted against d/λ, as shown in Figure 12b. Similar steady increase trend is observed, but the trend is not further observed for values of d/λ greater than 1.25. The relationship between the nonlinear parameter and d/λ can be further researched for indicating the debonding extent in a certain debonding range when the wavelength of the combined frequency wave is known. This is always the case since the input frequencies are always chosen in advance before conducting the tests.

7. CONCLUSION

Nonlinear Lamb wave mixing and its interaction with local debonding has been investigated in this paper using experiments and numerical simulations. It has been demonstrated that wave mixing technique can detect local debonding at adhesive metallic joints by observing generation of the combined frequency wave. The harmonics generated due to the contact effect

at the debonding have been extracted in the frequency domain for the experimental samples and used to validate the 3D FE model. The presence of the combined harmonic has been demonstrated to be effective and reliable for indicating local debonding. Furthermore, the effect of the debonding width has been investigated in the frequency domain given the complicated mechanisms when mixed frequency Lamb waves interacts with the damage. The numerical results have shown that the debonding width can be correlated with the energy generated due to debonding. This indicates that the proposed technique is also sensitive to different debonding widths within a specific range of d/λ. The study has also gained physical insight into the nonlinear Lamb wave mixing phenomena in adhesive joints. The findings presented can be used to further advance the debonding detection techniques using wave mixing.

REFERENCES

[1]   Piekarczyk M and Grec R 2012 Application of Adhesive Bonding in Steel and Aluminium Structures *Archives of Civil Engineering* **58**

[2]   Cavezza F, Boehm M, Terryn H, and Hauffman T 2020 A Review on Adhesively Bonded Aluminium Joints in the Automotive Industry *Metals* **10** 730

[3]   Chester R J, Walker K F, and Chalkley P D 1999 Adhesively bonded repairs to primary aircraft structure *International Journal of Adhesion and Adhesives* **19** 1-8

[4]   Lim H J, Kim J, Yang S, Sohn H, Bae I, and Jang J-H 2016 Development and field application of a nonlinear ultrasonic modulation technique for fatigue crack detection without reference data from an intact condition *Smart Materials and Structures* **25** 095055

[5]   Masserey B and Fromme P 2015 In-situ monitoring of fatigue crack growth using high frequency guided waves *NDT & E International* **71** 1-7

[6]   Giurgiutiu V, Zagrai A, and Jing Bao J 2002 Piezoelectric Wafer Embedded Active Sensors for Aging Aircraft Structural Health Monitoring *Structural Health Monitoring* **1** 41-61

[7]   Jhang K Y, *Overview—Nonlinear Ultrasonic Characteristics*, in *Measurement of Nonlinear Ultrasonic Characteristics*, K Y Jhang, et al., Editors. 2020, Springer: Singapore.

[8]   Chillara V and Lissenden C 2015 Review of nonlinear ultrasonic guided wave nondestructive evaluation: theory, numerics, and experiments *Optical Engineering* **55** 011002

[9]   Yeung C and Ng C T 2020 Nonlinear guided wave mixing in pipes for detection of material nonlinearity *Journal of Sound and Vibration* **485** 115541

[10]   Broda D, Staszewski W J, Martowicz A, Uhl T, and Silberschmidt V V 2014 Modelling of nonlinear crack–wave interactions for damage detection based on ultrasound—A review *Journal of Sound and Vibration* **333** 1097-1118

[11]   Solodov I Y, Krohn N, and Busse G 2002 CAN: an example of nonclassical acoustic nonlinearity in solids *Ultrasonics* **40** 621-625

[12]   Jhang K Y 2009 Nonlinear ultrasonic techniques for nondestructive assessment of micro damage in material: A review *International Journal of Precision Engineering and Manufacturing* **10** 123-135

[13]   Aseem A and Ng C T 2021 Debonding detection in rebar-reinforced concrete structures using second harmonic generation of longitudinal guided wave *NDT & E International* **122** 102496

[14]   Pruell C, Kim J Y, Qu J, and Jacobs L J 2009 A nonlinear-guided wave technique for evaluating plasticity-driven material damage in a metal plate *NDT & E International* **42** 199-203

[15]   Deng M and Pei J 2007 Assessment of accumulated fatigue damage in solid plates using nonlinear Lamb wave approach *Applied Physics Letters* **90** 121902

[16]   He S, Ng C T, and Yeung C 2020 Time-Domain Spectral Finite Element Method for Modeling Second Harmonic Generation of Guided Waves Induced by Material, Geometric and Contact Nonlinearities in Beams *International Journal of Structural Stability and Dynamics* **20** 2042005

[17]   Yang Y, Ng C T, Kotousov A, Sohn H, and Lim H J 2018 Second harmonic generation at fatigue cracks by low-frequency Lamb waves: Experimental and numerical studies *Mechanical Systems and Signal Processing* **99** 760-773

[18]   Yelve N, Mitra M, and Mujumdar P M 2017 Detection of delamination in composite laminates using Lamb wave based nonlinear method *Composite Structures* **159** 257-266

[19]   Soleimanpour R and Ng C T Scattering analysis of nonlinear Lamb waves at delaminations in composite laminates *Journal of Vibration and Control* **0** 1077546321990145

[20]   Yan D, Drinkwater B W, and Neild S A 2009 Measurement of the ultrasonic nonlinearity of kissing bonds in adhesive joints *NDT & E International* **42** 459-466

[21]   Mohseni H and Ng C T 2019 Rayleigh wave propagation and scattering characteristics at debondings in fibre-reinforced polymer-retrofitted concrete structures *Structural Health Monitoring* **18** 303-317

[22]   Shan S, Cheng L, and Li P 2016 Adhesive nonlinearity in Lamb-wave-based structural health monitoring systems *Smart Materials and Structures* **26** 025019

[23]   Van Den Abeele K E A, Johnson P A, and Sutin A 2000 Nonlinear Elastic Wave Spectroscopy (NEWS) Techniques to Discern Material Damage, Part I: Nonlinear Wave Modulation Spectroscopy (NWMS) *Research in Nondestructive Evaluation* **12** 17-30

[24]   Donskoy D, Ekimov A, Luzzato E, Lottiaux J-L, Stoupin S, and Zagrai A. *N-SCAN: new vibromodulation system for detection and monitoring of cracks and other contact-type defects*. in *Smart Structures and Materials*. 2003. SPIE.

[25]   Sun M, Xiang Y, Deng M, Tang B, Zhu W, and Xuan F-Z 2019 Experimental and numerical investigations of nonlinear interaction of counter-propagating Lamb waves *Applied Physics Letters* **114** 011902

[26]   Croxford A, Wilcox P D, Drinkwater B W, and Nagy P B 2009 The use of non-collinear mixing for nonlinear ultrasonic detection of plasticity and fatigue *The Journal of the Acoustical Society of America* **126** EL117-EL122

[27]   Jingpin J, Junjun S, Guanghai L, Bin W, and Cunfu H 2015 Evaluation of the intergranular corrosion in austenitic stainless steel using collinear wave mixing method *NDT & E International* **69** 1-8

[28]   Jingpin J, Junjun S, Nan L, Guorong S, Bin W, and Cunfu H 2014 Micro-crack detection using a collinear wave mixing technique *NDT & E International* **62** 122-129

[29]   Jingpin J, Hongtao L, Cunfu H, and Bin W 2017 Fatigue crack evaluation using the non-collinear wave mixing technique *Smart Materials and Structures* **26** 065005

[30]   Blanloeuil P, Meziane A, and Bacon C 2015 2D finite element modeling of the non-collinear mixing method for detection and characterization of closed cracks *NDT & E International* **76** 43-51

[31]   Joglekar D M and Mitra M 2017 Time domain analysis of nonlinear frequency mixing in a slender beam for localizing a breathing crack *Smart Materials and Structures* **26** 025009

[32]   Liu M and et al. 2012 Measuring acoustic nonlinearity parameter using collinear wave mixing *J. Appl. Phys.* **112** 24908

[33]   Tang G, Liu M, Jacobs L J, and Qu J 2014 Detecting Localized Plastic Strain by a Scanning Collinear Wave Mixing Method *Journal of Nondestructive Evaluation* **33** 196-204

[34]   Chen J, Su Z, and Cheng L 2009 Identification of corrosion damage in submerged structures using fundamental anti-symmetric Lamb waves *Smart Materials and Structures* **19** 015004

[35]   Sharma S and Mukherjee A 2015 Ultrasonic guided waves for monitoring corrosion in submerged plates *Structural Control and Health Monitoring* **22** 19-35

[36]   Aristégui C, Lowe M J S, and Cawley P 2001 Guided waves in fluid-filled pipes surrounded by different fluids *Ultrasonics* **39** 367-375

[37]   Hasanian M and Lissenden C 2017 Second order harmonic guided wave mutual interactions in plate: Vector analysis, numerical simulation, and experimental results *Journal of Applied Physics* **122** 084901

[38]   Hasanian M and Lissenden C 2018 Second order ultrasonic guided wave mutual interactions in plate: Arbitrary angles, internal resonance, and finite interaction region *Journal of Applied Physics* **124** 164904

[39]   Ishii Y, Hiraoka K, and Adachi T 2018 Finite-element analysis of non-collinear mixing of two lowest-order antisymmetric Rayleigh–Lamb waves *The Journal of the Acoustical Society of America* **144** 53-68

[40]   Chen H, Gao G, Hu N, Deng M, and Xiang Y 2020 Modeling and simulation of frequency mixing response of two counter-propagating Lamb waves in a two-layered plate *Ultrasonics* **104** 106109

[41]   Aslam M, Bijudas C R, Nagarajan P, and Remanan M 2020 Numerical and Experimental Investigation of Nonlinear Lamb Wave Mixing at Low Frequency *Journal of Aerospace Engineering* **33** 04020037

[42]   Li W, Deng M, Hu N, and Xiang Y 2018 Theoretical analysis and experimental observation of frequency mixing response of ultrasonic Lamb waves *Journal of Applied Physics* **124** 044901

[43]   Li W, Xu Y, Hu N, and Deng M 2019 Impact damage detection in composites using a guided wave mixing technique *Measurement Science and Technology* **31** 014001

[44]   Jingpin J, Xiangji M, Cunfu H, and Bin W 2017 Nonlinear Lamb wave-mixing technique for micro-crack detection in plates *NDT & E International* **85** 63-71

[45]   Metya A, Tarafder S, and Balasubramaniam K 2018 Nonlinear Lamb wave mixing for assessing localized deformation during creep *NDT & E International* **98** 89-94

[46]   Shan S and Cheng L 2020 Mode-mixing-induced second harmonic A0 mode Lamb wave for local incipient damage inspection *Smart Materials and Structures* **29** 055020

[47]   Ding X, Zhao Y, Deng M, Shui G, and Hu N 2020 One-way Lamb mixing method in thin plates with randomly distributed micro-cracks *International Journal of Mechanical Sciences* **171** 105371

[48]   Shan S, Hasanian M, Cho H, Lissenden C J, and Cheng L 2019 New nonlinear ultrasonic method for material characterization: Codirectional shear horizontal guided wave mixing in plate *Ultrasonics* **96** 64-74

[49]   Lowe M J S, Challis R E, and Chan C W 2000 The transmission of Lamb waves across adhesively bonded lap joints *The Journal of the Acoustical Society of America* **107** 1333-1345

[50]   Lanza di Scalea F, Rizzo P, and Marzani A 2004 Propagation of ultrasonic guided waves in lap-shear adhesive joints: Case of incident a0 Lamb wave *The Journal of the Acoustical Society of America* **115** 146-156

[51]   Wojtczak E and Rucka M 2019 Wave Frequency Effects on Damage Imaging in Adhesive Joints Using Lamb Waves and RMS *Materials* **12** 1842

[52]   Ramadas C, Balasubramaniam K, Joshi M, and Krishnamurthy C V 2009 Interaction of the primary anti-symmetric Lamb mode (Ao) with symmetric delaminations: numerical and experimental studies *Smart Materials and Structures* **18** 085011

[53]   Tian Z, Yu L, and Leckey C 2015 Delamination detection and quantification on laminated composite structures with Lamb waves and wavenumber analysis *Journal of Intelligent Material Systems and Structures* **26** 1723-1738

[54]   Koissin V, Demčenko A, and Korneev V A 2014 Isothermal epoxy-cure monitoring using nonlinear ultrasonics *International Journal of Adhesion and Adhesives* **52** 11-18

[55]   Escobar-Ruiz E, Ruiz A, Hassan W, Wright D, Collison I, Cawley P, and Nagy P 2014 Non-linear Ultrasonic NDE of Titanium Diffusion Bonds *Journal of Nondestructive Evaluation* **33** 187-195

[56]   Ju T, Achenbach J D, Jacobs L J, and Qu J 2019 Nondestructive evaluation of thermal aging of adhesive joints by using a nonlinear wave mixing technique *NDT & E International* **103** 62-67

[57]   de Lima W J N and Hamilton M F 2003 Finite-amplitude waves in isotropic elastic plates *Journal of Sound and Vibration* **265** 819-839

[58]   Alleyne D and Cawley P 1991 A two-dimensional Fourier transform method for the measurement of propagating multimode signals *The Journal of the Acoustical Society of America* **89** 1159-1168

[59]   Hu X, Ng C T, and Kotousov A 2021 Scattering characteristics of quasi-Scholte waves at blind holes in metallic plates with one side exposed to water *NDT & E International* **117** 102379

[60]   Yang Y, Ng C T, Mohabuth M, and Kotousov A 2019 Finite element prediction of acoustoelastic effect associated with Lamb wave propagation in pre-stressed plates *Smart Materials and Structures* **28** 095007

[61]   Willberg C, Duczek S, Vivar Perez J M, Schmicker D, and Gabbert U 2012 Comparison of different higher order finite element schemes for the simulation of Lamb waves *Computer Methods in Applied Mechanics and Engineering* **241-244** 246-261

[62]   Rajagopal P, Drozdz M, Skelton E A, Lowe M J S, and Craster R V 2012 On the use of absorbing layers to simulate the propagation of elastic waves in unbounded isotropic media using commercially available Finite Element packages *NDT & E International* **51** 30-40

[63]   Ng C T and Veidt M 2012 Scattering characteristics of Lamb waves from debondings at structural features in composite laminates *The Journal of the Acoustical Society of America* **132** 115-123

[64]   Diamanti K, Hodgkinson J M, and Soutis C 2004 Detection of Low-velocity Impact Damage in Composite Plates using Lamb Waves *Structural Health Monitoring* **3** 33-41

[65]   Lee Y, Lu Y, and Guan R 2020 Nonlinear guided waves for fatigue crack evaluation in steel joints with digital image correlation validation *Smart Materials and Structures* **29** 035031

[66]   Li B, Ye L, Li Z, Ma Z, and Kalhori H 2015 Quantitative identification of delamination at different interfaces using guided wave signals in composite laminates *Journal of Reinforced Plastics and Composites* **34** 1506-1525